Author Contributions:

Conceptualization: Narangoo Purevjav, Hongzhan Fei, Takayuki Ishii, Yanhao Lin, Ho-Kwang Mao, Tomoo Katsura
Formal analysis: Narangoo Purevjav, Hongzhan Fei, Giacomo Criniti
Investigation: Narangoo Purevjav, Hongzhan Fei
Methodology: Narangoo Purevjav, Hongzhan Fei
Supervision: Hongzhan Fei, Tomoo Katsura
Validation: Narangoo Purevjav
Visualization: Narangoo Purevjav
Writing – original draft: Narangoo Purevjav, Hongzhan Fei, Takayuki Ishii, Giacomo Criniti, Tomoo Katsura

Temperature Dependence of H$_2$O Solubility in Al-Free Stishovite

Narangoo Purevjav[1,2] , **Hongzhan Fei**[1,3] , **Takayuki Ishii**[1,4,5] , **Giacomo Criniti**[1] , **Yanhao Lin**[4], **Ho-Kwang Mao**[4], and **Tomoo Katsura**[1,4]

[1]Bayerisches Geoinstitut, University of Bayreuth, Bayreuth, Germany, [2]School of Earth and Environmental Sciences, Seoul National University, Seoul, Korea, [3]School of Earth Sciences, Zhejiang University, Hangzhou, China, [4]Center for High Pressure Science and Technology Advanced Research, Beijing, China, [5]Institute for Planetary Materials, Okayama University, Misasa, Japan

Abstract The role of stishovite in transporting water in subducting slabs has been a subject of debate for several decades. Here we investigated stishovite's water solubility and its potential role in water transportation as a function of temperature from 1300 to 2100°C at 22 GPa. Under water-saturated conditions, high-quality, Al-free stishovite single crystals were synthesized with multi-anvil press, and their water contents were measured using infrared spectroscopy. The H$_2$O solubility in stishovite increases from 128(20) to 521(47) wt. ppm with increasing temperature from 1300 to 1700°C and decreased to 145(26) wt. ppm at 2100°C. The maximum H$_2$O content was about seven times larger than earlier high-temperature multi-anvil studies but significantly lower than recent laser-heated diamond anvil cell and low-temperature multi-anvil studies. We suggest that Al-free stishovite may not be a significant H$_2$O carrier in subducting slabs, at least at the topmost lower mantle corresponding to our experimental conditions.

Plain Language Summary Stishovite is a high-pressure phase of silicon dioxide (SiO$_2$). It was recently reported that stishovite could contain a substantial amount of water based on diamond anvil cell experiments and, consequently, transport water into the lower mantle through subducting slabs. However, the water contents in their samples lack precise constrain due to the limited size of the recovered crystals, making them inaccessible for measurements using reliable FTIR spectroscopy or secondary-ion mass spectrometry. To settle this debate, we produced high-quality single crystals of stishovite under water-saturated conditions at high pressures and temperatures and measured their water contents using infrared spectroscopy. We discovered that stishovite contained only several hundred ppm of water under conditions at the top of the lower mantle. Therefore, it is likely that stishovite does not contain much water in the upper region of the lower mantle and does not transport water into the deep lower mantle.

1. Introduction

Subducted oceanic plates are expected to transport water into the deep mantle through hydrous and nominally anhydrous minerals (Hacker et al., 2003; Peslier et al., 2017; van Keken et al., 2011). The subducted slab is comprised of sedimentary, basaltic, and peridotitic layers. Lawsonite (8 GPa) and phengite (6 GPa) are likely the hydrous minerals in the sedimentary and basaltic layers (Poli & Schmidt, 2002; Schmidt & Poli, 1998). In the peridotitic layers, these minerals may include antigorite (~6 GPa) and dense hydrous magnesium silicates such as phase A (6–14 GPa), phase E (15 GPa), phase D (15–40 GPa), and 10 Å-phase (6.7 GPa) (Ohtani, 2015; Ono, 1998; Purevjav et al., 2020; Tomioka et al., 2016). However, these hydrous minerals are thermodynamically unstable at relatively high temperatures, i.e., >1300–1400°C (Ohtani, 2021). Consequently, they are likely to transport water only down to the mantle transition zone, which reaches the above-mentioned temperature limit (Tan et al., 2002).

In contrast, the dominant nominally anhydrous minerals in peridotite, such as olivine, wadsleyite, and ringwoodite, can incorporate up to ~30,000 wt. ppm of water as OH bonds within their crystal structures (Bolfan-Casanova, 2005; Demouchy et al., 2005; Fei et al., 2020; Fei & Katsura, 2020; Hirschmann et al., 2005; Kohlstedt et al., 1996; Purevjav et al., 2014, 2016, 2018; Smyth et al., 2006). Therefore, they may carry significant amounts of water down to the bottom of the mantle transition zone. This expectation has been supported by the discovery of hydrous ringwoodite and its decomposition products as diamond inclusions (Gu et al., 2022;

Writing – review & editing: Narangoo Purevjav, Hongzhan Fei, Takayuki Ishii, Giacomo Criniti, Tomoo Katsura

Pearson et al., 2014). However, the main minerals in the lower mantle, i.e., bridgmanite and ferropericlase, can only incorporate less than 1000 and 100 wt. ppm of water, respectively (e.g., Bolfan-Casanova et al., 2003; Fu et al., 2019; Liu et al., 2021; Purevjav et al., 2023). Therefore, the fate of the transported water to the lower mantle is unknown.

Even though the above argument is true for the peridotitic layer, which is made up of ultramafic systems, different minerals in the basaltic and sedimentary layers may be able to carry water because they are made up of more siliceous compositions. Particularly, stishovite, a high-pressure polymorph of silica occurring >10 GPa, constitutes approximately 20–25 vol.% and ~20 vol.% of mineral proportions in the basaltic and sedimentary layers, respectively (Ishii et al., 2012, 2019, Ishii, Miyajima, et al., 2022; Liu et al., 2019; Ono et al., 2001; Poli & Schmidt, 2002). It has been anticipated that stishovite could act as a water carrier into the lower mantle. However, studies on the water storage capacity of stishovite have yielded conflicting results. Earlier studies (Bromiley et al., 2006; Pawley et al., 1993) synthesized Al-free stishovite at 10–15 GPa and 1200–1500°C by multi-anvil experiments and found 3–7 wt. ppm of water in their samples through Fourier transform infrared (FTIR) spectroscopy. Additionally, Bolfan-Casanova et al. (2000) and Litasov et al. (2007) synthesized Al-free stishovite crystals at 15–24 GPa and 1200–1750°C, determining water contents of 16–72 wt. ppm via FTIR spectroscopy at ambient conditions. In contrast, recent multi-anvil experiments at relatively low pressure and temperature conditions by Spektor et al. (2011, 2016), Nisr, Leinenweber et al. (2017), and Nisr, Shim et al. (2017) reported up to 32,000 wt. ppm of water at 9–10 GPa and 350–550°C, where their water contents were determined using thermogravimetry analysis, secondary ion mass spectrometry, and unit-cell-volume expansion as determined by X-ray diffraction (XRD). It should be noted that although these studies reported significant amounts of water, their applicability is limited to the coldest slabs in relatively shallow regions. Under conditions of the deeper regions of the lower mantle, Lin et al. (2020, 2022) and Nisr et al. (2020) reported up to 100,000 wt. ppm of water in Al-free stishovite using a laser-heated diamond anvil cell (DAC), where water contents were estimated through unit-cell volume expansion as determined by XRD.

Thus, it remains unclear whether stishovite can exhibit significant water solubility and serve as an important water carrier in the deep mantle. To address this, we systematically investigated the water solubility in high-quality single crystals of Al-free stishovite as a function of temperature, ranging from 1300 to 2100°C, at a pressure of 22 GPa using the multi-anvil experimental technique and FTIR spectroscopy.

2. Sample Synthesis and Characterizations

2.1. Synthesis Experiments

The starting material was silica gel powder with a water content of 82,000 wt. ppm in all experiments. It was sealed by welding in Pt capsules with outer and inner diameters of 1.2 and 0.8 mm, respectively, and a length of 1.5 mm. The encapsulated starting material was loaded into a 10-mm 5% Cr_2O_3-bearing MgO octahedral pressure medium. A downscaled version of the zero-temperature gradient furnace developed by Zarei et al. (2018) was used to minimize the temperature uncertainty, estimated to be ±1°C. The cell assembly was pressurized to 22 GPa using a 12-MN Kawai-type multi-anvil apparatus with inner tungsten carbide anvils with 4-mm truncations at the Bayerisches Geoinstitut, University of Bayreuth (Keppler & Frost, 2005). The sample was then heated to the target temperatures (1300–2100°C) for 4–20 hr while being monitored by a D-type ($W_{97}Re_3/W_{75}Re_{25}$) thermocouple without calibration of the pressure effect. Note that different heating durations were employed to facilitate the growth of large single crystals. As long as thermodynamic equilibrium was reached in each run, the water contents in the stishovite samples are not affected by the heating duration. Finally, heating was terminated cutting off the power supply, and the sample was then decompressed to ambient pressure.

2.2. Characterization of Recovered Products

The sample capsules were recovered from the assemblies, and holes were created in their walls to confirm the presence of liquid water inside the capsules. Subsequently, the sample capsules were embedded in epoxy resin to make cross-sections with polished surfaces for characterization. The compositions of crystals were measured using an energy-dispersive spectrometer (EDS) to confirm chemical homogeneity. All the crystals were then separated from the capsules for further characterization. Several crystals from each run were selected for the determination of their unit-cell parameters using a Huber single-crystal X-ray diffractometer equipped with

Table 1
Details of the Synthesis Runs and the Unit-Cell Parameters of Stishovite

Run No	Temperature (°C)	Duration (hr)	Products	H_2O (wt. ppm)[a]	Unit-cell parameters (Å) a	Unit-cell parameters (Å) c	Volume (Å³)	No of reflections
H5630	1300	15	St + fluid	128(20)	4.1785(2)	2.6660(2)	46.549(5)	15
H5326	1500	5	St + fluid	315(53)	4.1783(6)	2.6667(8)	46.56(2)	14
H5486	1700	20	St + fluid	521(47)	4.1784(1)	2.6656(1)	46.540(4)	29
H5312[b]	1800	5	St + fluid	340(10)[b]	–	–	–	–
H5376	1900	5	St + fluid	293(18)	4.1786(1)	2.6658(1)	46.546(2)	31
H5592[c]	2100[d]	4	St + melt	145(26)	4.1785(3)	2.6658(3)	46.544(8)	29

[a]H_2O contents were determined by averaging the H_2O contents determined by unpolarized spectra of several different grains from the same batch. Uncertainties in the H_2O content are one standard deviation of the water content. [b]Since H5312 was not measured by single-crystal X-ray diffractometry, the density of H5376 was used for calculating the H_2O content of it using Paterson's (1982) equation. [c]Phase E powder was found in the capsule, suggesting MgO contamination during loading the silica gel powder into the capsule. Nevertheless, EDS analysis showed no detectable amount of MgO in the stishovite crystals. [d]The synthesis temperature was estimated by a temperature-power relationship from other runs. St denotes stishovite.

Mo$K\alpha$ radiation and a point detector driven by the software SINGLE (Angel & Finger, 2011). The unit-cell parameters of each crystal were determined through a vector least-square inversion involving 14–31 reflections (Table 1), each centered in eight equivalent positions (King & Finger, 1979; Ralph & Finger, 1982).

2.3. Water Content Determination

The water contents in the recovered crystals were determined using a Bruker IFS 120 HR high-resolution FTIR spectrometer coupled with a Bruker IR microscope. Measurements were conducted using a tungsten light source, a CaF$_2$ beamsplitter, and a high-sensitivity narrow-band MCT (mercury-cadmium-telluride) detector cooled by liquid nitrogen. Two or three crystals from each run were selected for unpolarized FTIR measurements, and these crystals were not exposed to scanning electron microscopy (SEM). They were polished on both sides to a thickness of 80–100 μm for unpolarized FTIR measurements. Each spectrum was obtained using an unpolarized infrared beam with a diameter of 20–50 μm by accumulating 100 scans with a resolution of 2 cm^{-1}. Three to five spectra were obtained from each crystal. Prior to measuring each sample, a background of the spectrum was collected using the same aperture settings without the sample.

The water contents were calculated from unpolarized spectra using the calibration of Paterson (1982),

$$C_{OH} = \frac{Xi}{150\zeta} \int \frac{K(\overline{v})}{(3780 - \overline{v})} d\overline{v} \tag{1}$$

where C_{OH} is the water content in wt. ppm, ζ is an orientation factor, 1/3 for unpolarized spectra, $K(\overline{v})$ is the absorption coefficient in cm^{-1} for the given wavenumber $\overline{v}$, and Xi is the density factor determined as $Xi = 10^6 \times (18/2d)$, where d is the density of stishovite (in g/l). The d of each run was calculated using the lattice volume determined by the single-crystal X-ray diffraction, as shown in Table 1. To apply Equation 1, each spectrum was numerically integrated with wavenumbers between $\overline{v}$ 2,600 and 3,400 cm^{-1}.

3. Results

3.1. Run Products

Liquid water was observed to leak from the capsules when pierced with a needle after recovery from high-pressure and high-temperature conditions, confirming that all experiments were conducted under water-saturated conditions. Crystals ranging in size from 50 to 400 μm, as well as cavities, were found in the capsules using optical microscopy. The recovered crystals appeared transparent without visible inclusions. Backscattered electron images of the capsule cross-sections also revealed the presence of large crystals and cavities (Figure 1). Micro-focused X-ray diffraction analysis indicated that the crystals possessed a stishovite structure. It is worth
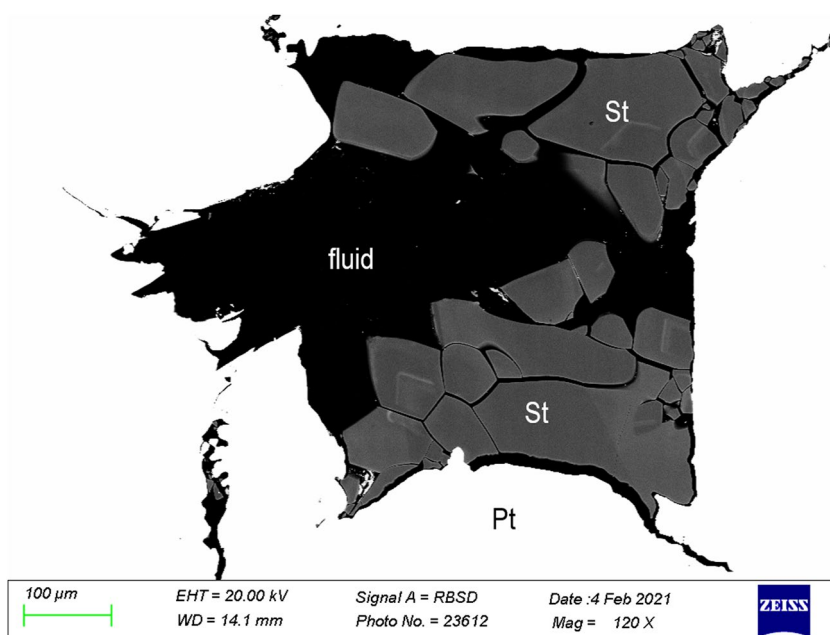
Figure 1. A backscattered electron image of a cross-section of the sample synthesized at 22 GPa and 1900°C in the Pt capsule (H5376). The crystal sizes are ∼100–200 μm. A cavity is seen within the capsule, where a fluid is expected to have existed before recovery. St and Pt denote stishovite and platinum, respectively.

noting that due to the large size of the recovered stishovite crystals and the small diameter of the X-ray beam used, only a few crystals were exposed to the X-ray beam. Consequently, only a few bright spots were observed in X-ray images instead of diffraction rings. Nevertheless, the observed diffraction angles perfectly matched those expected for SiO_2 stishovite (Sinclair & Ringwood, 1978). In run H5592, stishovite crystals were recovered alongside phase E powder, suggesting sample contamination by MgO. We consider that phase E formed upon quenching a hydrous melt. EDS indicated that the crystals of stishovite were made of pure SiO_2. Even in sample H5592, no detectable amount of MgO was identified (Table S1 in Supporting Information S1). Within the mutual uncertainties, single-crystal XRD measurements revealed identical unit-cell parameters of all samples. No distortion to post-stishovite was observed, unlike in hydrous Al-bearing samples recovered from similar pressure-temperature conditions (Ishii, Criniti, et al., 2022). Single-crystal XRD also revealed that the crystals from each run exhibited very sharp and narrow peaks, with full width half maxima of <0.06° measured on omega scans, confirming the high degree of crystallinity of the stishovite samples.
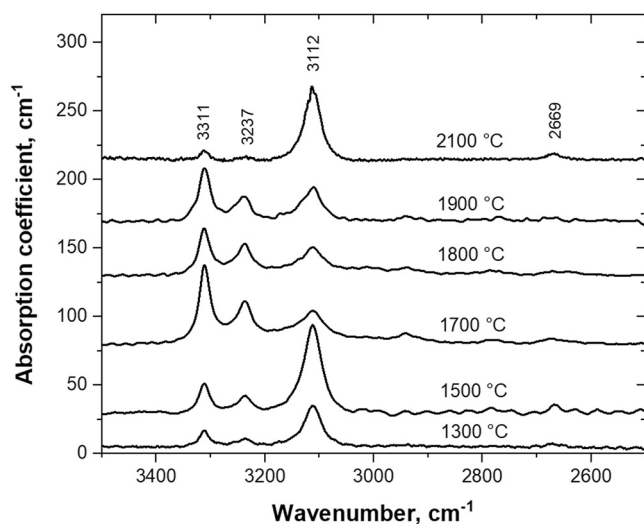
3.2. Infrared Spectra and Water Contents in Stishovite Crystals

Unpolarized spectra of Al-free stishovite synthesized at 22 GPa exhibit four OH bands at 2,669, 3,112, 3,237, and 3,311 cm^{-1} (Figure 2). These bands were consistent with previously reported OH bands in Al-free stishovite. Particularly, the shape of the unpolarized spectra of 1300, 1500, and 2100°C resembles that of the unpolarized spectra of previous multi-anvil studies (Bromiley et al., 2006; Litasov et al., 2007), which were reported to contain <40 wt. ppm H_2O. The OH band at 3,112 cm^{-1} was the most intense in their spectra, as observed in our stishovite spectra for 1300, 1500, and 2100°C runs, suggesting that this OH band is the most pronounced at low water content. In contrast to previous studies, the OH band at 3,312 cm^{-1} was the most intense in stishovite synthesized at 1700°C with 521(47) wt. ppm H_2O. The intensity of the OH band at 3,312 cm^{-1} was found to increase with the highest water content and start to

Figure 2. Representative unpolarized spectra of stishovite synthesized at 22 GPa and 1300–2100°C. All spectra are baseline subtracted and thickness normalized. Spectra are vertically shifted for visibility.
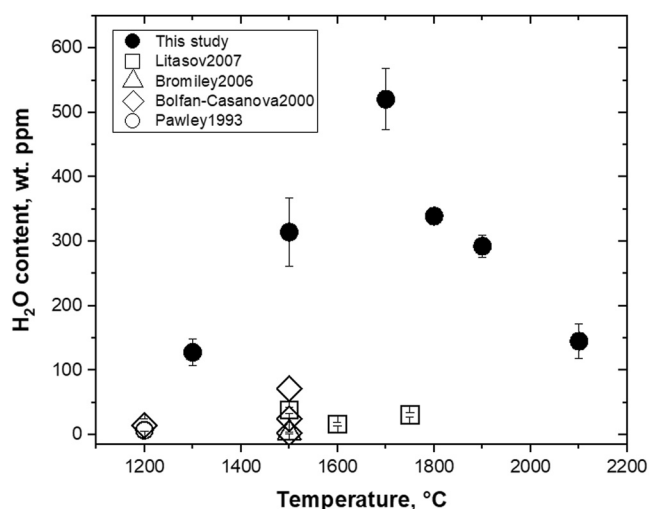
Figure 3. Temperature dependence of H₂O content in stishovite. The black circles are from this study, and squares, triangles, diamonds, and open circles are from Litasov et al. (2007), Bromiley et al. (2006), Bolfan-Casanova et al. (2000), and Pawley et al. (1993), respectively. Note that the experiments of Bromiley et al. (2006) and Pawley et al. (1993) were carried out at 15 and 10 GPa, and the experiments of Bolfan-Casanova et al. (2000) and Litasov et al. (2007) were carried out at 15–21 GPa and 20 and 24 GPa.

decrease with decreasing water content. Thus, we suggest that the increase in water content enhances the prominence of the OH band at 3,312 cm^{-1}.

The determined H$_2$O contents were consistent between different spectra obtained from a single grain and also between different grains from the same capsule batch. The FTIR spectra displayed reproducibility within and between the grains, indicating a homogenous water distribution within the crystals. Figure 3 illustrates the stishovite water content as a function of temperature. The water content increases with increasing temperature up to 1700°C but decreases above this temperature. The highest water content was 521(47) wt. ppm at 1700°C, while the lowest was 128(20) wt. ppm at 1300°C. We conducted a second water content measurement for stishovite from run H5486 three months after the initial analysis. The first and second measurements yielded water content values of 518(49) and 521(47) wt. ppm, respectively, indicating no water loss from the crystals after recovery.

4. Discussion

4.1. Comparison With Previous Studies

A positive temperature dependence of water content of stishovite was observed at temperatures below 1700°C. The maximum water content measured in Al-free stishovite in this study was 521(47) wt. ppm at 1700°C and 22 GPa. This amount is significantly higher than the results reported by Pawley et al. (1993) and Bromiley et al. (2006), who reported <7 wt. ppm H$_2$O at 10–15 GPa and 1200–1500°C (Table S2 in Supporting Information S1). This difference can be attributed to pressure variance, as increasing pressure elevates water fugacity, enhancing the water solubility in nominally anhydrous minerals (Mosenfelder, 2000; Mosenfelder et al., 2006; Smyth et al., 2006). Our reported 521(47) wt. ppm H$_2$O is considerably higher than that of the 16–72 wt. ppm H$_2$O reported by Bolfan-Casanova et al. (2000) and Litasov et al. (2007) at 15–24 GPa and 1200–1750°C (Figure 3). Since two phases, stishovite and fluid, coexisted in the SiO$_2$–H$_2$O binary system in our experiments, the water content in stishovite should be uniquely determined according to the phase rule. In contrast, Litasov et al. (2007) observed stishovite crystals coexisting with hydrous silicate melts containing Fe$_x$O, K$_2$O, CO$_2$, and MgO, which may not have reached maximum water content due to additional degrees of freedom. Specifically, water activity should be close to unity in our experiments, as we observed H$_2$O-fluid phases. However, the water content in the hydrous silicate melt in a complex system is only 150,000–250,000 wt. ppm at 1600–1800°C (Fei, 2021), and therefore, the water activity in Litasov et al. (2007)'s study should be much lower than in this study. This may explain the difference in water content between Litasov et al. (2007) and our results.

The highest water content value obtained in the current study was significantly lower than that of the multi-anvil studies performed at lower pressure and temperature than those in this study (Nisr, Leinenweber et al., 2017; Nisr, Shim et al., 2017; Spektor et al., 2011, 2016 (Table S2 in Supporting Information S1)). The OH bands of infrared spectra reported by Spektor et al. (2011, 2016) are significantly broader than those of our current and previous multi-anvil studies at higher temperatures. They reported three OH bands at 2,644, 2,884, and 3,388 cm^{-1} and elaborated that the two OH bands at lower frequencies are due to the substitution of octahedral hydrogarnet defects (4H$^+$ for 1Si^{4+}), and the later OH band at 3,388 cm^{-1} is grain boundary water. Their OH band at 2,644 cm^{-1} are comparable to our OH band at 2,669 cm^{-1}, while the rest of the OH bands are very different. They used Libowitzky's (1999) correlation of OH frequencies with O–H…O distances to explain that the two lower OH-band frequencies are due to the hydrogen between the two longer oxygens (O–O distances are 2.57 and 2.66 Å). We also correlated our OH band frequencies to the above-mentioned correlation. It was found that our OH band frequencies from 2669 to 3,311 cm^{-1} all correspond to the two longer O–O distances, 2.57 and 2.66 Å. Therefore, we consider that the difference in IR absorption band characteristics between the current study and Spektor et al. (2011, 2016) may be due to the different hydrogen bond configurations in the stishovite structure. Although the hydrogen is incorporated via the 4H$^+$ for 1Si^{4+} mechanism, the hydrogen bond configuration may be different between lower pressure and temperature conditions and higher pressure and temperature conditions. This may also explain the discrepancies in water content between the current study and Spektor

et al. (2011, 2016). Since our experimental conditions cover a wide range of temperatures at the topmost lower mantle, the results should be applicable to the subducting slabs and ambient mantle near the 660 km discontinuity.

Lin et al. (2020, 2022) and Nisr et al. (2020) determined the water contents in stishovite at much higher pressures (>33 GPa) than the current study (22 GPa) based on the expansion of unit-cell-volume using DAC experiments and synchrotron XRD. They reported that the Al-free stishovite can uptake up to 100,000 wt. ppm of H_2O. Their experiments were conducted at significantly higher pressures than the current study. Therefore, the difference in water content between the current study and theirs could be due to the pressure effect, where the water solubility of stishovite may have increased significantly at high pressures. Another explanation for the discrepancy might be the much higher differential stresses in the DAC experiments, which may cause high dislocation density. High-density dislocations and stacking faults may have trapped considerable amounts of water and enlarged the apparent unit-cell volumes. In addition, Lin et al. (2020) reported water loss during the decompression process at ~10 GPa. If the crystal initially had high water content and was lost upon decompression, this could result in the formation of water inclusion since hydrogen diffusion kinetics at room temperature are insufficient for water to escape from the crystal. Subsequently, substantial amounts of water inclusions must be formed. However, we did not observe any broad infrared absorption bands at wavenumber of about 3,400 cm^{-1} (Figure 2) or through the petrographic microscope. Therefore, water loss during decompression should be insignificant in our experiments.

4.2. Temperature Dependence of H_2O Solubility in Stishovite

Our results indicate that the H_2O solubility in Al-free stishovite increases with increasing temperature up to 1700°C, but the water solubility decreases with increasing temperature >1700°C. Such a phenomenon is also observed in olivine: the water solubility in olivine increases with increasing temperature below 1250°C, but decreases with increasing temperature >1250°C (Bali et al., 2008; Smyth et al., 2006). We assume that the peak of the H_2O solubility result forms two factors in the activity term of the chemical potential of the water fluid. The chemical potentials of the stishovite and the fluid can be expressed as:

$$\mu_{H_2O}^{St} = \mu_{H_2O}^{St\,°} + RT \ln a_{H_2O}^{St} \tag{2}$$

$$\mu_{H_2O}^{Fl} = \mu_{H_2O}^{Fl\,°} + RT \ln a_{H_2O}^{Fl} \tag{3}$$

where $\mu_{H_2O}^{M}$ is the chemical potential of the H_2O component in the phase M, $\mu_{H_2O}^{M\,°}$ is the chemical potential of H_2O in the pure phase M, and a is the activity of the H_2O component in the phase M. R is the gas constant, and T is the temperature. St and Fl denote the stishovite and the fluid, respectively.

Under equilibrium conditions, we have $\mu_{H_2O}^{St} = \mu_{H_2O}^{Fl}$. Therefore, based on Equations 2 and 3, the water activity in stishovite, $a_{H_2O}^{St}$, which should be linearly proportional to the water content in stishovite, can be expressed as:

$$a_{H_2O}^{St} = a_{H_2O}^{Fl} \exp\left(-\frac{\mu_{H_2O}^{St\,°} - \mu_{H_2O}^{Fl\,°}}{RT}\right) \tag{4}$$

The $a_{H_2O}^{Fl}$ is expected to decrease with increasing temperature, thus decreasing $a_{H_2O}^{St}$. On the other hand, since the pure H_2O fluid should be more stable than the pure H_2O stishovite, $\mu_{H_2O}^{St\,°} - \mu_{H_2O}^{Fl\,°}$ should be positive. As a result, the exponent becomes close to zero with increasing temperature. The product of these two opposite temperature dependencies produces the solubility peak. Although, in reality, the solid/fluid ratio is constant at low temperatures because the fluid is always close to pure water, increasing temperature will increase the water activity, resulting in an increase in the water content of stishovite. At high temperatures, the fluid becomes melt. The melt fraction increases significantly with increasing temperature because SiO_2 dissolves into water; as a result, the water content in the melt decreases.

4.3. Geophysical Implications

The pyrolytic mantle is ultramafic, and thus the majority of the lower mantle does not contain stishovite. However, the basaltic and sedimentary layers of subducted oceanic crusts are enriched in silica, stishovite is formed as these

materials are recycled into the mantle transition zone and lower mantle (Ishii et al., 2019; Ishii, Miyajima, 2022; Liu et al., 2019). Silica components in crusts can be either Al-bearing (e.g., lawsonite and phengite) or almost pure SiO_2 minerals (e.g., quartz and chalcedony). Consequently, they will form Al-bearing and Al-free stishovite, respectively, in the subducted crusts. Even though the exact ratio of Al-bearing and Al-free stishovite is unknown, both of these minerals have been thought to be important for transporting water from shallow regions to the deep mantle (Lin et al., 2020, 2022; Lin & Mao, 2022; Nisr et al., 2020). However, such a conclusion should be reconsidered according to our experimental results.

Since our experimental temperatures cover the geotherm from cold slabs to hot ambient mantle at ~660 km depth, the water solubility found in this study should represent the maximum water content in Al-free stishovite at the temperature of the bottom of the mantle transition zone and topmost lower mantle. Therefore, Al-free stishovite can carry at most 521 wt. ppm of water into the lower mantle. Although this value is much higher than that of ferropericlase (<10 wt. ppm) (Bolfan-Casanova et al., 2000; Joachim et al., 2013), it is only slightly higher, or even comparable to those of bridgmanite and davemaoite (Fu et al., 2019; Liu et al., 2021; Németh et al., 2017; Purevjav et al., 2023), and much lower than that of majorite (1130–1250 wt. ppm) (Katayama et al., 2003). Therefore, Al-free stishovite cannot be the dominant water carrier from the upper mantle to the topmost lower mantle.

It should be noted that some slabs, such as the Tonga and Java slabs, may have extremely low geotherms, less than 1000°C at 660 km depth (Kaneshima & Yoshioka, 2014; King et al., 2015). The positive temperature dependence of water solubility obtained in this study suggests that stishovite contains less than 50 wt. ppm of water in such cold slabs near 660 km depth. Although slab temperature will gradually increase during descent, it should always be lower than the ambient mantle, and therefore, the water content in stishovite should be limited. Of course, it is theoretically possible that the hydrogen substitution mechanism in stishovite might be different at temperatures below this study (<1300°C), resulting in different temperature dependencies on water solubility. Further multi-anvil experiments are essential to constrain the water content of stishovite in extremely cold slabs.

In the case of the Al-bearing system, Al_2O_3 content in stishovite increases with pressure (Litasov & Ohtani, 2005; Liu et al., 2019), and thus its water content may increase due to the coupling of aluminum and hydrogen incorporation. Recently, it was found that Al-bearing silica in $CaCl_2$-structured stishovite, i.e., post-stishovite, can contain up to ~11,000 wt. ppm at 24–28 GPa and 1000–2000°C (Ishii, Criniti, et al., 2022), corresponding to the topmost lower mantle conditions. Therefore, we can still consider Al-bearing stishovite as a potential water carrier in the topmost lower mantle.

Data Availability Statement

All the raw FTIR and microfocused XRD data are archived in Zenodo (Purevjav et al., 2024).

References

Angel, R. J., & Finger, L. W. (2011). SINGLE: A program to control single-crystal diffractometers. *Journal of Applied Crystallography*, *44*(1), 247–251. https://doi.org/10.1107/S0021889810042305

Bali, E., Bolfan-Casanova, N., & Koga, K. T. (2008). Pressure and temperature dependence of H solubility in forsterite: An implication to water activity in the Earth interior. *Earth and Planetary Science Letters*, *268*(3–4), 354–363. https://doi.org/10.1016/j.epsl.2008.01.035

Bolfan-Casanova, N. (2005). Water in the Earth's mantle. *Mineralogical Magazine*, *69*(3), 229–257. https://doi.org/10.1180/0026461056930248

Bolfan-Casanova, N., Keppler, H., & Rubie, D. C. (2000). Water partitioning between nominally anhydrous minerals in the MgO-SiO_2-H_2O system up to 24 GPa: Implications for the distribution of water in the Earth's mantle. *Earth and Planetary Science Letters*, *182*(3–4), 209–221. https://doi.org/10.1016/S0012-821X(00)00244-2

Bolfan-Casanova, N., Keppler, H., & Rubie, D. C. (2003). Water partitioning at 660 km depth and evidence for very low water solubility in magnesium silicate perovskite. *Geophysical Research Letters*, *30*(17), 1–4. https://doi.org/10.1029/2003GL017182

Bromiley, G. D., Bromiley, F. A., & Bromiley, D. W. (2006). On the mechanisms for H and Al incorporation in stishovite. *Physics and Chemistry of Minerals*, *33*(8–9), 613–621. https://doi.org/10.1007/s00269-006-0107-9

Demouchy, S., Deloule, E., Frost, D. J., & Keppler, H. (2005). Pressure and temperature-dependence of water solubility in Fe-free wadsleyite. *American Mineralogist*, *90*(7), 1084–1091. https://doi.org/10.2138/am.2005.1751

Fei, H. (2021). Water content of the dehydration melting layer in the topmost lower mantle. *Geophysical Research Letters*, *48*(1), 1–10. https://doi.org/10.1029/2020GL090973

Fei, H., Druzhbin, D., & Katsura, T. (2020). The effect of water on ionic conductivity in olivine. *Journal of Geophysical Research: Solid Earth*, *125*(3), e2019JB019313. https://doi.org/10.1029/2019JB019313

Fei, H., & Katsura, T. (2020). Pressure dependence of proton incorporation and water solubility in olivine. *Journal of Geophysical Research: Solid Earth*, *125*(2), 1–13. https://doi.org/10.1029/2019JB018813

Fu, S., Yang, J., Karato, S. I., Vasiliev, A., Presniakov, M. Y., Gavrilliuk, A. G., et al. (2019). Water concentration in single-crystal (Al,Fe)-bearing bridgmanite grown from the hydrous melt: Implications for dehydration melting at the topmost lower mantle. *Geophysical Research Letters*, *46*(17–18), 10346–10357. https://doi.org/10.1029/2019GL084630

Gu, T., Pamato, M. G., Novella, D., Alvaro, M., Fournelle, J., Brenker, F. E., et al. (2022). Hydrous peridotitic fragments of Earth's mantle 660 km discontinuity sampled by a diamond. *Nature Geoscience*, *15*(11), 950–954. https://doi.org/10.1038/s41561-022-01024-y

Hacker, B. R., Peacock, S. M., Abers, G. A., & Holloway, S. D. (2003). Subduction factory 2. Are intermediate-depth earthquakes in subducting slabs linked to metamorphic dehydration reactions? *Journal of Geophysical Research*, *108*(B1), 2030. https://doi.org/10.1029/2001jb001129

Hirschmann, M. M., Aubaud, C., & Withers, A. C. (2005). Storage capacity of H_2O in nominally anhydrous minerals in the upper mantle. *Earth and Planetary Science Letters*, *236*(1–2), 167–181. https://doi.org/10.1016/j.epsl.2005.04.022

Ishii, T., Criniti, G., Ohtani, E., Purevjav, N., Fei, H., Katsura, T., & Mao, H. K. (2022). Superhydrous aluminous silica phases as major water hosts in high-temperature lower mantle. *Proceedings of the National Academy of Sciences*, *119*(44), e2211243119. https://doi.org/10.1073/PNAS.2211243119

Ishii, T., Kojitani, H., & Akaogi, M. (2012). High-pressure phase transitions and subduction behavior of continental crust at pressure-temperature conditions up to the upper part of the lower mantle. *Earth and Planetary Science Letters*, *357–358*, 31–41. https://doi.org/10.1016/j.epsl.2012.09.019

Ishii, T., Kojitani, H., & Akaogi, M. (2019). Phase relations of harzburgite and MORB up to the uppermost lower mantle conditions: Precise comparison with pyrolite by multisample cell high-pressure experiments with implication to dynamics of subducted slabs. *Journal of Geophysical Research: Solid Earth*, *124*(4), 3491–3507. https://doi.org/10.1029/2018JB016749

Ishii, T., Miyajima, N., Criniti, G., Hu, Q., Glazyrin, K., & Katsura, T. (2022). High pressure-temperature phase relations of basaltic crust up to mid-mantle conditions. *Earth and Planetary Science Letters*, *584*, 117472. https://doi.org/10.1016/J.EPSL.2022.117472

Joachim, B., Wohlers, A., Norberg, N., Gardés, E., Petrishcheva, E., & Abart, R. (2013). Diffusion and solubility of hydrogen and water in periclase. *Physics and Chemistry of Minerals*, *40*(1), 19–27. https://doi.org/10.1007/s00269-012-0542-8

Kaneshima, S., & Yoshioka, S. (2014). Dominant role of temperature on deep earthquake mechanics for the Tonga slab near the bottom of the upper mantle. *Planets and Space*, *66*(1), 138. https://doi.org/10.1186/s40623-014-0138-2

Katayama, I., Hirose, K., Yurimoto, H., & Nakashima, S. (2003). Water solubility in majoritic garnet in subducting oceanic crust. *Geophysical Research Letters*, *30*(22), 5–8. https://doi.org/10.1029/2003GL018127

Keppler, H., & Frost, D. J. (2005). Introduction to minerals under extreme conditions, *Mineral behaviour at extreme conditions* (Vol. 7), European Mineralogical Union. https://doi.org/10.1180/EMU-notes.7.1

King, H. E., & Finger, L. W. (1979). Diffracted beam crystal centering and its application to high-pressure crystallography. *Journal of Applied Crystallography*, *12*(4), 374–378. https://doi.org/10.1107/s0021889879012723

King, S. D., Frost, D. J., & Rubie, D. C. (2015). Why cold slabs stagnate in the transition zone. *Geology*, *43*(3), 231–234. https://doi.org/10.1130/G36320.1

Kohlstedt, D. L., Keppler, H., & Rubie, D. C. (1996). Solubility of water in the α, β and γ phases of $(Mg,Fe)_2SiO_4$. *Contributions to Mineralogy and Petrology*, *123*(4), 345–357. https://doi.org/10.1007/s004100050161

Libowitzky, E. (1999). Correlation of O–H stretching frequencies and O–H O hydrogen bond lengths in minerals. *Monatshefte Fur Chemie*, *130*(8), 1047–1059. https://doi.org/10.1007/BF03354882

Lin, Y., Hu, Q., Meng, Y., Walter, M., & Mao, H. K. (2020). Evidence for the stability of ultrahydrous stishovite in Earth's lower mantle. *Proceedings of the National Academy of Sciences of the United States of America*, *117*(1), 184–189. https://doi.org/10.1073/pnas.1914295117

Lin, Y., Hu, Q., Yang, J., Meng, Y., Zhuang, Y., Mao, H.-K., et al. (2022). Hydrous SiO_2 in subducted oceanic crust and water transport to the core-mantle boundary. *Earth and Planetary Science Letters*, *594*, 117708. https://doi.org/10.1016/j.epsl.2022.117708

Lin, Y., & Mao, H. K. (2022). Dense hydrous silica carrying water to the deep Earth and promotion of oxygen fugacity heterogeneity. *Matter and Radiation at Extremes*, *7*(6), 068101. https://doi.org/10.1063/5.0125744

Litasov, K. D., Kagi, H., Shatskiy, A., Ohtani, E., Lakshtanov, D. L., Bass, J. D., & Ito, E. (2007). High hydrogen solubility in Al-rich stishovite and water transport in the lower mantle. *Earth and Planetary Science Letters*, *262*(3–4), 620–634. https://doi.org/10.1016/j.epsl.2007.08.015

Litasov, K. D., & Ohtani, E. (2005). Phase relations in hydrous MORB at 18-28 GPa: Implications for heterogeneity of the lower mantle. *Physics of the Earth and Planetary Interiors*, *150*(4), 239–263. https://doi.org/10.1016/j.pepi.2004.10.010

Liu, X., Matsukage, K. N., Nishihara, Y., Suzuki, T., & Takahashi, E. (2019). Stability of the hydrous phases of Al-rich phase D and Al-rich phase H in deep subducted oceanic crust. *American Mineralogist*, *104*(1), 64–72. https://doi.org/10.2138/am-2019-6559

Liu, Z., Fei, H., Chen, L., McCammon, C., Wang, L., Liu, R., et al. (2021). Bridgmanite is nearly dry at the top of the lower mantle. *Earth and Planetary Science Letters*, *570*, 117088. https://doi.org/10.1016/j.epsl.2021.117088

Mosenfelder, J. L. (2000). Pressure dependence of hydroxyl solubility in coesite. *Physics and Chemistry of Minerals*, *27*(9), 610–617. https://doi.org/10.1007/s002690000105

Mosenfelder, J. L., Deligne, N. I., Asimow, P. D., & Rossman, G. R. (2006). Hydrogen incorporation in olivine from 2-12 GPa. *American Mineralogist*, *91*(2–3), 285–294. https://doi.org/10.2138/am.2006.1943

Németh, P., Leinenweber, K., Ohfuji, H., Groy, T., Domanik, K. J., Kovács, I. J., et al. (2017). Water-bearing, high-pressure Ca-silicates. *Earth and Planetary Science Letters*, *469*, 148–155. https://doi.org/10.1016/j.epsl.2017.04.011

Nisr, C., Chen, H., Leinenweber, K., Chizmeshya, A., Prakapenka, V. B., Prescher, C., et al. (2020). Large H_2O solubility in dense silica and its implications for the interiors of water-rich planets. *Proceedings of the National Academy of Sciences of the United States of America*, *117*(18), 9747–9754. https://doi.org/10.1073/pnas.1917448117

Nisr, C., Leinenweber, K., Prakapenka, V., Prescher, C., Tkachev, S., & Shim, S. H. D. (2017). Phase transition and equation of state of dense hydrous silica up to 63 GPa. *Journal of Geophysical Research: Solid Earth*, *122*(9), 6972–6983. https://doi.org/10.1002/2017JB014055

Nisr, C., Shim, S. H., Leinenweber, K., & Chizmeshya, A. (2017). Raman spectroscopy of water-rich stishovite and dense high-pressure silica up to 55 GPa. *American Mineralogist*, *102*(11), 2180–2189. https://doi.org/10.2138/am-2017-5944

Ohtani, E. (2015). Hydrous minerals and the storage of water in the deep mantle. *Chemical Geology*, *418*, 6–15. https://doi.org/10.1016/j.chemgeo.2015.05.005

Ohtani, E. (2021). Hydration and dehydration in Earth's interior. *Annual Review of Earth and Planetary Sciences*, *49*(1), 253–278. https://doi.org/10.1146/annurev-earth-080320-062509

Ono, S. (1998). Stability limits of hydrous minerals in sediment and mid-ocean ridge basalt compositions: Implications for water transport in subduction zones. *Journal of Geophysical Research*, *103*(8), 18253–18267. https://doi.org/10.1029/98jb01351

Ono, S., Ito, E., & Katsura, T. (2001). Mineralogy of subducted basaltic crust (MORB) from 25 to 37 GPa, and chemical heterogeneity of the lower mantle. *Earth and Planetary Science Letters*, *190*(1–2), 57–63. https://doi.org/10.1016/S0012-821X(01)00375-2

Paterson, M. S. (1982). The determination of hydroxyl by infrared adsorption in quartz, silicate glasses and similar materials. *Bulletin de Minéralogie*, *105*(1), 20–29. https://doi.org/10.3406/bulmi.1982.7582

Pawley, A. R., McMillan, P. F., & Holloway, J. R. (1993). Hydrogen in stishovite, with implications for mantle water content. *Science*, *261*(5124), 1024–1026. https://doi.org/10.1126/science.261.5124.1024

Pearson, D. G., Brenker, F. E., Nestola, F., McNeill, J., Nasdala, L., Hutchison, M. T., et al. (2014). Hydrous mantle transition zone indicated by ringwoodite included within diamond. *Nature*, *507*(7491), 221–224. https://doi.org/10.1038/nature13080

Peslier, A. H., Schönbächler, M., Busemann, H., & Karato, S. I. (2017). Water in the Earth's interior: Distribution and origin. *Space Science Reviews*, *212*(1–2), 743–810. https://doi.org/10.1007/s11214-017-0387-z

Poli, S., & Schmidt, M. W. (2002). Petrology of subducted slabs. *Annual Review of Earth and Planetary Sciences*, *30*(1), 207–235. https://doi.org/10.1146/annurev.earth.30.091201.140550

Purevjav, N., Fei, H., Ishii, T., Criniti, G., Lin, Y., Mao, H.-K., & Katsura, T. (2024). Supporting data for "Temperature dependence of H_2O solubility in Al-free stishovite" [Dataset]. Zenodo. https://doi.org/10.5281/zenodo.10478661

Purevjav, N., Okuchi, T., & Hoffmann, C. (2020). Strong hydrogen bonding in a dense hydrous magnesium silicate discovered by neutron Laue diffraction. *IUCrJ*, *7*(3), 370–374. https://doi.org/10.1107/S2052252520003036

Purevjav, N., Okuchi, T., Tomioka, N., Abe, J., & Harjo, S. (2014). Hydrogen site analysis of hydrous ringwoodite in mantle transition zone by pulsed neutron diffraction. *Geophysical Research Letters*, *41*(19), 6718–6724. https://doi.org/10.1002/2014GL061448

Purevjav, N., Okuchi, T., Tomioka, N., Wang, X., & Hoffmann, C. (2016). Quantitative analysis of hydrogen sites and occupancy in deep mantle hydrous wadsleyite using single crystal neutron diffraction. *Scientific Reports*, *6*, 1–8. https://doi.org/10.1038/srep34988

Purevjav, N., Okuchi, T., Wang, X., Hoffmann, C., & Tomioka, N. (2018). Determination of hydrogen site and occupancy in hydrous Mg_2SiO_4 spinel by single-crystal neutron diffraction. *Acta Crystallographica Section B: Structural Science, Crystal Engineering and Materials*, *74*(1), 115–120. https://doi.org/10.1107/S2052520618000616

Purevjav, N., Tomioka, N., Yamashita, S., Shinoda, K., Kobayashi, S., Shimizu, K., et al. (2023). Hydrogen incorporation mechanism in the lower-mantle bridgmanite. *American Mineralogist*. in press. https://doi.org/10.2138/am-2022-8680

Ralph, R. L., & Finger, L. W. (1982). (IUCr) A computer program for refinement of crystal orientation matrix and lattice constants from diffractometer data with lattice symmetry constraints. *Journal of Applied Crystallography*, *15*(5), 537–539. https://doi.org/10.1107/S0021889882012539

Schmidt, M. W., & Poli, S. (1998). Experimentally based water budgets for dehydrating slabs and consequences for arc magma generation. *Earth and Planetary Science Letters*, *163*(1–4), 361–379. https://doi.org/10.1016/S0012-821X(98)00142-3

Sinclair, W., & Ringwood, A. E. (1978). Single crystal analysis of the structure of stishovite. *Nature (London, United Kingdom)*, *272*(5655), 714–715. https://doi.org/10.1038/272714a0

Smyth, J. R., Frost, D. J., Nestola, F., Holl, C. M., & Bromiley, G. (2006). Olivine hydration in the deep upper mantle: Effects of temperature and silica activity. *Geophysical Research Letters*, *33*(15), L15301. https://doi.org/10.1029/2006GL026194

Spektor, K., Nylen, J., Mathew, R., Edén, M., Stoyanov, E., Navrotsky, A., et al. (2016). Formation of hydrous stishovite from coesite in high-pressure hydrothermal environments. *American Mineralogist*, *101*(11), 2514–2524. https://doi.org/10.2138/am-2016-5609

Spektor, K., Nylen, J., Stoyanov, E., Navrotsky, A., Hervig, R. L., Leinenweber, K., et al. (2011). Ultrahydrous stishovite from high-pressure hydrothermal treatment of SiO_2. *Proceedings of the National Academy of Sciences of the United States of America*, *108*(52), 20918–20922. https://doi.org/10.1073/pnas.1117152108

Tan, E., Gurnis, M., & Han, L. (2002). Slabs in the lower mantle and their modulation of plume formation. *Geochemistry, Geophysics, Geosystems*, *3*(11), 1–24. https://doi.org/10.1029/2001gc000238

Tomioka, N., Okuchi, T., Purevjav, N., Abe, J., & Harjo, S. (2016). Hydrogen sites in the dense hydrous magnesian silicate phase E: A pulsed neutron powder diffraction study. *Physics and Chemistry of Minerals*, *43*(4), 267–275. https://doi.org/10.1007/s00269-015-0791-4

van Keken, P. E., Hacker, B. R., Syracuse, E. M., & Abers, G. A. (2011). Subduction factory: 4. Depth-dependent flux of H_2O from subducting slabs worldwide. *Journal of Geophysical Research*, *116*(1), B01401. https://doi.org/10.1029/2010JB007922

Zarei, A., Li, Y., Fei, H., & Katsura, T. (2018). A nearly zero temperature gradient furnace system for high pressure multi-anvil experiments. *High Pressure Research*, *38*(3), 243–249. https://doi.org/10.1080/08957959.2018.1479851